

***In vivo* three-dimensional radiopharmaceutical excited fluorescence tomography**

**Zhenhua Hu<sup>1,2,+</sup>, Mingxuan Zhao<sup>3,+</sup>, Yawei Qu<sup>4,+</sup>, Xiaojun Zhang<sup>5,+</sup>, Mingru Zhang<sup>3</sup>,  
Muhan Liu<sup>1</sup>, Hongbo Guo<sup>1</sup>, Zeyu Zhang<sup>1</sup>, Jing Wang<sup>3,\*</sup>, Weidong Yang<sup>3,\*</sup>, and Jie  
Tian<sup>1,2,\*</sup>**

<sup>1</sup>*Key Laboratory of Molecular Imaging of Chinese Academy of Sciences, Institute of  
Automation, Chinese Academy of Sciences, Beijing, 100190, China*

<sup>2</sup>*The State Key Laboratory of Management and Control for Complex Systems, Institute of  
Automation, Chinese Academy of Sciences, Beijing 100190, China*

<sup>3</sup>*Department of Nuclear Medicine, Xijing Hospital, Fourth Military Medical University,  
Xi'an, 710032, China*

<sup>4</sup>*Department of Gastroenterology, General Hospital of Chinese Armed Police Forces,  
Beijing, 100039, China*

<sup>5</sup>*Department of Nuclear Medicine, Chinese PLA General Hospital, Beijing, 100853,  
China*

<sup>+</sup>These authors contributed equally to this work.

<sup>\*</sup>Corresponding author: wangjing@fmmu.edu.cn (Jing Wang), *Department of Nuclear  
Medicine, Xijing Hospital, Fourth Military Medical University, Xi'an 710032, China*;  
yangwd1971@163.com (Weidong Yang), *Department of Nuclear Medicine, Xijing  
Hospital, Fourth Military Medical University, Xi'an 710032, China*; tian@ieee.org (Jie  
Tian), *Key Laboratory of Molecular Imaging of Chinese Academy of Sciences, Institute of  
Automation, Chinese Academy of Sciences, Beijing, 100190, China*

Word count: 4862 words

## ABSTRACT

Cerenkov luminescence imaging (CLI) can image radiopharmaceuticals using high-sensitivity charge coupled device (CCD) camera. However, Cerenkov luminescence (CL) emitted from the radiopharmaceuticals is weak and has low penetration depth in biological tissues, which severely limits the sensitivity and accuracy of CLI. This study presents the three-dimensional (3D) radiopharmaceutical excited fluorescence tomography (REFT) using europium oxide (EO) nanoparticles, which enhances the CL signal intensity, improves the penetration depth, and obtains more accurate 3D distribution of radiopharmaceuticals. **Methods:** The enhanced optical signals of various radiopharmaceuticals (including  $\text{Na}^{131}\text{I}$ ,  $^{18}\text{F}$ -FDG,  $^{68}\text{GaCl}_3$ ,  $\text{Na}^{99\text{m}}\text{TcO}_4$ ) by EO nanoparticles were detected *in vitro*. The location and 3D distribution of the radiopharmaceuticals of REFT were then reconstructed and compared with those of Cerenkov luminescence tomography (CLT) through the experiments of the phantom, artificial source-implanted mouse models, and mice bearing hepatocellular carcinomas (HCCs). **Results:** The mixture of  $^{68}\text{GaCl}_3$  and EO nanoparticles possessed the strongest optical signals compared with the other mixtures. The *in vitro* phantom and implanted mouse studies showed that REFT revealed more accurate 3D distribution of  $^{68}\text{GaCl}_3$ . REFT can detect more tumors than small animal positron emission tomography (PET) in HCC bearing mice and achieved more accurate 3D distribution information compared with CLT. **Conclusion:** REFT with EO nanoparticles significantly improves accuracy of localization of radiopharmaceuticals and can precisely localize the tumor *in vivo*.

**Key Words:** radiopharmaceutical excitation fluorescence tomography (REFT); Cerenkov luminescence imaging (CLI); radionuclides; hepatocellular carcinoma (HCC); PET

## INTRODUCTION

Cerenkov luminescence imaging (CLI) provides a convenient approach to image the *in vivo* distribution of radiopharmaceuticals using optical instruments. It has attracted lots of attentions and been widely applied in animals imaging<sup>[1-9]</sup>. Compared with the positron emitting tomography (PET) or single photon emission computed tomography (SPECT), CLI has several distinctive advantages, such as high throughput, cost savings and the ability of imaging therapeutic pure beta emitters. Recently, human thyroid gland of a patient treated orally with Na<sup>131</sup>I has been successfully imaged with CLI<sup>[10]</sup>. The patients' lymphatic nodes in the axillary region have also been visualized with CLI by injection of <sup>18</sup>F-fluorodeoxyglucose (<sup>18</sup>F-FDG)<sup>[11]</sup>. However, the emission of Cerenkov radiance dominantly distributes in the blue-violet light region (300-500 nm), which results in great absorption in biological tissues and low penetration depth<sup>[2,8]</sup>. This severely limits the broad applications and potential clinical translation ability of CLI. To resolve these problems, researchers have tried to design new instruments<sup>[11-13]</sup> and explore creative ways to transfer or enhance the Cerenkov signal for better detection<sup>[14-16]</sup>. Liu *et al.* have developed a Cerenkov luminescence endoscopy system, which has potential to image abnormalities inside the human body<sup>[11]</sup>. On the other hand, Cerenkov radiance energy transfer (CRET) has demonstrated that Cerenkov radiance can excite a variety of fluorophores such as quantum dots (QDs) to emit light with longer wavelengths<sup>[14-16]</sup>. More importantly, Thorek *et al.* show that the secondary Cerenkov induced fluorescence imaging effectively reduces the optical signal of the non-target tissues and improves the target-to-background tissues ratios<sup>[17]</sup>.

CLI is the two-dimensional planar imaging modality which simply provides the qualitative information and only reflects whether there are luminescent signal in the target of the interest. Three-dimensional (3D) Cerenkov luminescence tomography (CLT) provides more information, such as the specific location of the lesion, depth, and size<sup>[18-23]</sup>, which is important for diagnosis and treatment of disease. However, the reconstruction of CLT usually are not very accurate<sup>[18-23]</sup>, which is caused by the following three elements: the inaccuracy of the photon transport model and reconstruction algorithm, the limitation of the surface luminescent signal detected by CCD with much random noise and weak intensity, and the deviation from data processing, such as the registration and segmentation.

In this study, a novel 3D radiopharmaceuticals excited fluorescence tomography (REFT) has been developed to improve the reconstruction of CLT. REFT has been explored based on our previous work on the novel radiopharmaceuticals excited fluorescence imaging (REFI) technique that can dramatically enhance the signal intensity using the dual excitation of nanoparticles by both gamma rays and CL<sup>[24]</sup>. Combining the anatomical information provided by computed tomography (CT), REFT can realize 3D visualization and distribution information and improve the CLT reconstruction by increasing the intensity and signal to noise ratio (SNR) of surface fluorescent signal. Specifically, in this study, the enhancement of the optical signal of a variety of

radiopharmaceuticals by EO nanoparticles was tested. REFT for phantoms, artificial source-implantation mouse models, and tumor xenograft mouse models was conducted and compared with CLT. Furthermore, the performance of REFT in tumor detection was evaluated through the comparison with CLT and small animal PET.

## **MATERIALS AND METHODS**

### **Preparation of radiopharmaceuticals and europium oxide nanoparticles**

Radiopharmaceuticals including  $\text{Na}^{131}\text{I}$ ,  $^{18}\text{F}$ -FDG,  $^{68}\text{GaCl}_3$ , and  $\text{Na}^{99\text{m}}\text{TcO}_4$  for this study were obtained from the Department of Nuclear Medicine, Xijing Hospital, the Fourth Military Medical University (FMMU). The europium oxide (EO) nanoparticle ( $\text{Eu}_2\text{O}_3$ , 99.9% metal basis, molecular weight = 351.91) was purchased from Aladdin Reagents (Shanghai) Co. Ltd. and used as previously described<sup>[24]</sup>. The excitation spectrum and emission spectrum of EO nanoparticles were recorded with a fluorescence spectrophotometer (F-4500, Hitachi, Japan).

### ***In vitro* optical imaging of radiopharmaceuticals and EO nanoparticles**

In the first experiment, EO nanoparticles (100  $\mu\text{L}$ , 2 mg/mL) were added into the wells of the black 96-well plates and the optical images were acquired without any excitation. In the second experiment,  $\text{Na}^{131}\text{I}$ ,  $^{18}\text{F}$ -FDG,  $^{68}\text{GaCl}_3$ , or  $\text{Na}^{99\text{m}}\text{TcO}_4$  (10  $\mu\text{Ci}$  in 50  $\mu\text{L}$ ) alone or mixed with 50  $\mu\text{L}$  (2 mg/mL) of EO nanoparticles respectively were added into the wells of the black 96-well plates. In the third experiment,  $^{18}\text{F}$ -FDG (10  $\mu\text{Ci}$  in 100  $\mu\text{L}$ ) and the mixture of  $^{18}\text{F}$ -FDG (10  $\mu\text{Ci}$  or 20  $\mu\text{Ci}$  in 50  $\mu\text{L}$ ) and EO nanoparticles (50  $\mu\text{L}$ , 2 mg/mL) were added into the wells of the black 96-well plates. All optical images were acquired with IVIS Kinetic imaging system (PerkinElmer). For all the experiments, images were acquired with an  $8 \times 8$  binning, aperture  $f_{\text{num}}$  of 1 and 1 minute exposure time for *in vitro* imaging and 5 minutes for *in vivo* imaging. No filter was used and net photon production was collected to compare the intensities of CL and radiopharmaceutical excited fluorescence (radiofluorescence). Regions of interest (ROIs) of the corresponding areas were drawn over the optical images of the optical sources, and the average radiances were calculated by the Living Image 3.2 software (PerkinElmer), which provided the quantification information such as intensities of the optical signals.

### **Optical imaging of EO nanoparticles excited by $^{68}\text{GaCl}_3$**

Firstly, CLI for 100  $\mu\text{L}$  of  $^{68}\text{GaCl}_3$  with various activities (1.25  $\mu\text{Ci}$ , 2.5  $\mu\text{Ci}$ , 5  $\mu\text{Ci}$ , 10  $\mu\text{Ci}$  and 20  $\mu\text{Ci}$ ) were performed. Secondly, REFI of 50  $\mu\text{L}$  of EO (20 mg/mL) excited by 50  $\mu\text{L}$  of  $^{68}\text{GaCl}_3$  with various activities (1.25  $\mu\text{Ci}$ , 2.5  $\mu\text{Ci}$ , 5  $\mu\text{Ci}$ , 10  $\mu\text{Ci}$  and 20  $\mu\text{Ci}$ ) were carried. Thirdly, REFI for 10  $\mu\text{Ci}$   $^{68}\text{GaCl}_3$  in 50  $\mu\text{L}$  mixed with 50  $\mu\text{L}$  of EO with various concentrations (2.5 mg/mL, 5 mg/mL, 10 mg/mL, 20 mg/mL and 40 mg/mL) were studied.

### **Phantom imaging for CLT and REFT comparison**

*Ex vivo phantom experiment.* Cubic phantoms were used to mimic the biological tissue in *ex vivo* phantom study. The phantom was made from polyethylene and has sides of length 40 mm. The refractive index of the phantom was 1.5. Circular holes of diameter 2.3 mm and various depths from the top surface of the phantom were drilled to place  $^{68}\text{GaCl}_3$  or the mixture of  $^{68}\text{GaCl}_3$  and EO. The five phantoms contained 5  $\mu\text{Ci}$   $^{68}\text{GaCl}_3$  (5  $\mu\text{L}$ ) at the bottom of the holes were used for CLT experiments. The mixture of 5  $\mu\text{Ci}$   $^{68}\text{GaCl}_3$  (5  $\mu\text{L}$ ) and 1 mg EO was used for REFT experiments. The depths of the sources were 1 mm, 2 mm, 5 mm, 7 mm and 8 mm, respectively. The heights of the cylindrical solution were 2 mm.

*In vivo phantom experiment.* To investigate the performance of REFT in the real biological application, an artificial source-implantation study on living animals was performed. All animals were obtained from the Laboratory Animal Center of the FMMU, and all animal studies were conducted in compliance with the FMMU Animal Studies Committee (Protocol 20090260).  $^{68}\text{GaCl}_3$  (100  $\mu\text{Ci}$ , 5  $\mu\text{L}$ ) was mixed with 20  $\mu\text{L}$  of EO (100 mg/mL) in a microfuge tube. Anesthetized male athymic Balb/c mice (n=9) between the age of 6-7 weeks underwent aseptic celiotomy and were implanted with the microfuge tubes at different positions in the abdominal cavity. The embedded artificial sources were positioned close to the ventral surface of the abdomen, the lesser curvature of the stomach and the dorsal surface of the abdomen of the mice, respectively (n=3 for each position). Similarly, the mice (n=9) were implanted with sources contained only  $^{68}\text{GaCl}_3$  (100  $\mu\text{Ci}$ , 5  $\mu\text{L}$ ) as the control group. After implantation, mice immediately underwent REFT and CLT.

### **Orthotopic and ectopic xenografts of HCC tumor**

Well-differentiated luciferase labelled human hepatocellular carcinoma (HCC) cells HepG2-Red-Fluc (PerkinElmer, BW134280) was used to construct tumor models. Male athymic Balb/c nude mice (n=4) between the ages of 6-7 weeks were injected with  $5 \times 10^6$  HCC cells dispensed in 30  $\mu\text{L}$  of matrigel into the liver lobes and the peritoneum. All of them developed tumors and used for the study. Two weeks later, the HCC tumor bearing mice were subjected to *in vivo* imaging studies.

### **X-ray computed tomography imaging**

Our previously developed micro-CT system was used to provide structural information for optical source reconstruction in imaging of phantoms and xenografts<sup>[18]</sup>. The scanner operated at 55 kVp and 145  $\mu\text{A}$ . For *in vivo* imaging of mouse models, mice were fixed on a holder and anesthetized by inhalation of a 1%–2% isoflurane-oxygen mixture. No contrast agent was used.

### ***Ex vivo* and *in vivo* REFT imaging**

In *ex vivo* phantom imaging experiments, CLI and REFI images were acquired and then the phantoms underwent CT scans as described above. The images were registered

to segmented CT volumes of the cubic phantoms and optical source reconstruction was performed.

In *in vivo* phantom imaging, mice were anesthetized by inhalation of a 1–2% isoflurane-oxygen mixture and fixed on a holder. CLI and REFI images were acquired followed by CT scans. The images were registered to segmented CT volumes of the mice and optical source reconstruction was performed.

In xenograft imaging experiments, mice bearing HCC tumors were fasted overnight before the injection of  $^{18}\text{F}$ -FDG (60  $\mu\text{Ci}$ , 0.1 mL) intravenously. CLI and PET scans (using a GENISYS4 scanner, Sofie Biosciences) were performed. 10-minute static scan mode was used. Then the mice were injected with EO nanoparticles (0.1 mL, 1 mg/mL) intravenously and REFI images were acquired. After CLI, PET scans and REFI, the mice were undergone CT scan.

### REFT source reconstruction method

To reconstruct the 3D distribution of the radiofluorescence, the Cerenkov radiation spectral characteristic-based source reconstruction method was used in the REFT<sup>[22]</sup>.

Based on this method, the relationship between the radiofluorescence source and surface flux density can be established as follows:

$$\tilde{H}_j C_j^q = \tilde{\Psi}_j^A \quad (1)$$

where  $\tilde{H}_j$  is the system matrix for the  $j$ -th level mesh which is related to the estimated optical properties;  $C_j^q$  denotes the radiofluorescence distribution located in the permissible source region that is determined by *a priori* knowledge; and  $\tilde{\Psi}_j^A$  represents the nodal flux density on the mouse surface obtained without any filters.

It is difficult to solve Eq. (1) directly because of the ill-posed nature of the internal source reconstruction. The classical conjugate gradient least squares (CGLS) can be employed to solve the Eq. (1). The following optimization problem is defined to determine the 3D radiofluorescence distribution:

$$\min_{C_{\text{inf}} \leq C_j^q \leq C_{\text{sup}}} \Theta(C_j^q) = \left\| \tilde{H}_j C_j^q - \tilde{\Psi}_j^A \right\|_{L^2(\Omega)} + \lambda_j \left\| C_j^q \right\|_{L^2(\Omega)} \quad (2)$$

where  $C_{\text{inf}}$  and  $C_{\text{sup}}$  are the lower and upper bounds of the radiofluorescence power density and  $\lambda_j$  represents the regularization parameter.  $L^2(\Omega)$  denotes the weight matrix and satisfies  $\|V\|_{L^2(\Omega)} = V^T L^2(\Omega) V$ .

### Statistical Analysis

Data were expressed as mean  $\pm$  SD. Statistical significance was determined using the Student *t* test (v6.0, GraphPad Prism software). Linear regression was determined using Origin software for Windows (v8.0, Origin Pro software). Differences between groups were considered significant if  $P \leq 0.05$ .

## RESULTS

### Excitation spectrum and emission spectrum of EO nanoparticles

The excitation spectrum is shown in Fig. S1a. There were multiple characteristic absorption peaks at 363, 382, 394, 466 and 535 nm. The peak of emission spectrum of EO nanoparticles was 613 nm (Fig. S1b).

### EO emitted the highest radiofluorescence when excited by $^{68}\text{GaCl}_3$

There was no any light of EO nanoparticles without excitation (Fig. 1a). The optical signal intensities dramatically increased after mixing the radiopharmaceuticals with EO nanoparticles, and the mixture of  $^{68}\text{GaCl}_3$  and EO nanoparticles possessed the strongest optical intensity (Fig. 1b). The increased optical signal intensity of mixture of  $^{68}\text{GaCl}_3$  and EO nanoparticles was the maximum compared with other mixtures (Fig. 1c). Compared with CL signal of  $^{18}\text{F}$ -FDG, the REF signal of the mixture of  $^{18}\text{F}$ -FDG and EO nanoparticles was obviously enhanced (Fig. 1d).

### Optical signal intensity of REFI increased with radioactivity of $^{68}\text{GaCl}_3$ and concentration of EO nanoparticles

The REF signal increased with radioactivity of  $^{68}\text{GaCl}_3$  and concentration of EO (Fig. S2a). The quantification relationship between REF intensity and radioactivity, and concentration of EO is shown in Fig. S2b and c, respectively. The excited REF signal intensity linearly correlated with radioactivity of  $^{68}\text{GaCl}_3$  ( $y=1.5e^7+1.9e^6x$ ,  $R^2=0.96$ ) and the concentration of EO ( $y=1.86e^6+9.96e^5x$ ,  $R^2=0.98$ ), respectively.

### REFT improved the accuracy of reconstruction results

The total flux of signal of  $^{68}\text{GaCl}_3$  penetrated through 1 mm of phantom material was  $6.55 \times 10^6$  photons/s. It decreased to  $4.38 \times 10^6$  photons/s through 5 mm (Fig. 2a). However the total signal of EO excited by  $^{68}\text{GaCl}_3$  was much more intense than CL signal of  $^{68}\text{GaCl}_3$ , and the signal of EO mixed with  $^{68}\text{GaCl}_3$  was  $6.53 \times 10^7$  photons/s through 1 mm, and decreased to  $3.79 \times 10^7$  photons/s (8.65 times to that of  $^{68}\text{GaCl}_3$ ) through 5 mm (Fig. 2b). REF signals were significantly higher than CL ( $P<0.05$ ) (Fig. 2c). Although the reconstructed distance error increased with the increase of the source depth, which was observed both in CLT and REFT, the reconstruction results of REFT were more accurate than those of the CLT (Fig. 2d). For example, the reconstructed position of EO excited by  $^{68}\text{GaCl}_3$  was 1.89 mm away from the actual position in depth of 5 mm, but it was 2.62 mm for  $^{68}\text{GaCl}_3$  alone.

### **Comparison of CLT and REFT on artificial source-implanted mouse**

The radionuclide source with or without EO were implanted with different depths in the mouse separately, followed by REFI (Fig. 3a, left) and CLI (Fig. 3a, right) detection. The first row of the implanted source was only 0.77 mm to the ventral surface of the mice, the second was closed to the lesser curvature and 6.11 mm to the ventral surface, the third was closed to the dorsal surface and 13.47 mm to the dorsal surface (Fig. 3a). Fig. 3b shows the comparison of reconstruction results of REFT (left) and CLT (right) of the implanted sources. Obviously the reconstructed distance error (DE) increased with the source depth. When the depth of the implanted source was 0.77 mm, the reconstructed DE of CLT and REFT was 1.84 mm and 1.35 mm, respectively. When the implanted source depth was 13.47 mm, DE of CLT and REFT was 7.85 mm and 2.85 mm, respectively. Furthermore, for the different source depths, all the results of REFT were more accurate than that of CLT. Fig. 3c further shows the relationship between the reconstructed DE of REFT or CLT and the depth of the implanted source. Again the reconstructed DE increased with the depth. More importantly, the reconstructed DE of REFT was less than that of CLT, indicating that REFT can localize the implanted source more accurate than that of CLT.

### **REFT of mice bearing HCC tumors**

Interestingly in the experiment, PET imaging only delineated a tumor in abdominal (red arrow in Fig. 4a). CLI of the same mouse showed that there were more optical signals in several locations. It detected three tumors (red arrows in Fig. 4b) especially in the lower abdomen, but CL of the upper two tumors was almost too weak to be detected. Three tumors were also detected by REFI (Fig. 4c), and REFT delineated the 3D positions of the tumors more clearly (Fig. 4d). Fig. 4e further displayed the axial, coronal and sagittal image of the tumor presented in the lower abdomen region (yellow arrows). The distribution of  $^{18}\text{F}$ -FDG uptake in the tumor was clearly visualized. After imaging, the mouse was dissected and the photograph of the three tumors during the operation of the mouse is shown in Fig. 4f. The locations of the tumors were consistence with the findings as revealed by REFT, as indicated by the yellow arrows. All three dissected tumors were confirmed with H&E (Fig. 4g). This study showed that REFT provided 3D visualization which not only clearly detected more tumors but also localized the tumors more accurately.

In the experiment, four orthotropic and ectopic HCC tumor-bearing mice were used to perform REFT and PET. The comparison of detection rates was also listed in the Table 1. The experimental results showed that REFT detected significantly more tumors than that of PET (detection rate:  $88.75\pm 13.15\%$  vs.  $42.08\pm 15.84\%$ ,  $P<0.05$ ).

## **DISCUSSION**

This study presents a novel three-dimensional (3D) REFT imaging technique for *in vivo* imaging of tumor mice. The most important advantages of REFT include that: 1) it can

obtain 3D visualization information of tumors with a small deviation of reconstructed location; 2) it can more clearly and easily detect tumors than other methods such as CLT; 3) it has strong capability in reconstructing the deeper source in living animals. In the phantom and the implanted mice experiment, we have found that the radiopharmaceutical excited fluorescence can penetrate more than 12 mm in the real biological tissues (Fig. 3). REFT shows high potential of imaging deep tumors. Furthermore, from 1 mm to 13 mm of the light source, REFT results are more accurate and robust than that of CLT, as shown in Fig. 2d and Fig. 3c. Although distance error of REFT or CLT increases with the increasing the source depth, in 12 mm case the reconstruction error of REFT is only about 3 mm which is much smaller than the reconstruction error of CLT with 8 mm. The significant improved reconstruction results of REFT is likely due to the following reasons. The greater tissue attenuation of the lower wavelength spectrum generated by Cerenkov photon results in the higher background noise compared to the narrow peak from the nanoparticle (hence greater penetration). On the other hand, the signal intensity of REFT is stronger than that of CLT due to the energy transfer from the gamma rays and Cerenkov light. Therefore, the signal-to-noise ratio of REFT is higher than that of CLT.

CLT reconstruction with multispectral images is time consuming, and an accurate reconstruction result with little time cost has been successfully achieved in this study. This is mainly attributed to that the ill-posed problem of the source reconstruction has been improved by using a greater number of surface measurement data with less random noise and more strong optical signals. Moreover, the classical CGLS technique has been employed in our current work to reconstruct the sources [22]. In the axial image in Fig. 4e (axial), it looks like two lesions. The weak signal shown in the right side of lesion could be a small metastasis that was not delineated by CLI and REFI. This could open new opportunities for using REFT for imaging ultra-small lesions and is worthy of further investigations.

The phantom experiment and artificial source-implanted mouse of REFT have clearly proven the reliability and accuracy of REFT. We further conducted the imaging study of orthotropic and ectopic HCC tumor-bearing mice. The small animal-PET only detected one tumor in the mouse abdomen. CLI detected three tumors (indicated by red arrows in Fig. 4b). However CL of the upper two tumors was almost too weak to be detected by CLI. As a comparison, REFI imaging has identified three tumors in the mouse. However the other useful and important information such as the location, depth and size of the tumors cannot be obtained. To address this issue, REFT has been developed and evaluated in this study. It is clearly that REFT not only can light up all the three tumors but also accurately locate them in the mouse. The tumor specific anatomical position has testified the accuracy of REFT. Overall, these results have demonstrated that the proposed novel 3D REFT imaging technique can better detect tumor and achieve 3D visualization and distribution information compared with CLI and REFI, which is crucial to the diagnosis and treatment of disease.

In this experiment, REFT detected all three HCC tumors, and PET only detected one

tumor. The possible explanation for this observation is that different microenvironment of tumor cell may lead to different level of  $^{18}\text{F}$ -FDG uptake. PET picked up the tumor which had the highest  $^{18}\text{F}$ -FDG accumulation among the three tumors. The other two tumors may uptake less of  $^{18}\text{F}$ -FDG which beyond the detection sensitivity of PET. In contrast, the optical signal intensities of all the three tumors were enhanced greatly and thus they were successfully detected with REFT technique. This result suggests that REFT could be more efficient than PET in detecting tumor in some circumstances. More studies using different types of tumors and probes would be helpful to further evaluate and clarify this observation.

Compared with the CLI, REFI signal is significantly enhanced for most of radiopharmaceuticals in this study. Since the mixture of  $^{68}\text{GaCl}_3$  and EO nanoparticles displays the highest optical signal, it has been chosen to conduct the consecutive phantom and implantable experiments. The specific reasons for highest imaging sensitivity of  $^{68}\text{GaCl}_3$  may be related to its decay scheme, branching ratio and energy spectrum of decay products. Although  $^{68}\text{GaCl}_3$  is an ideal radionuclide for REFT, it lacks of suitable  $^{68}\text{Ga}$ -based targeting probe for HCC, and  $^{18}\text{F}$ -FDG was thus used in animal tumor imaging. In the future study, we will further explore  $^{68}\text{GaCl}_3$  labeled probes for imaging other type of tumors, such as  $^{68}\text{Ga}$ -DOTA-TATE for neuroendocrine tumor imaging. It should also be noted that the clinical translation of EO nanoparticles can be problematic. Novel nanoparticles with higher biocompatibility are desired to be used for REFT. But overall, our study highlights the potential advantages of REFT. With the advancement of material science, REFT may be eventually translated into clinical use.

## CONCLUSION

Signal of CL of radiopharmaceuticals and its tissue penetration can be dramatically enhanced by EO. 3D REFT with EO nanoparticles significant improves accuracy of localization of radiopharmaceuticals and can also precisely localize the tumor *in vivo*.

## ACKNOWLEDGMENTS

This study was supported by the National Natural Science Foundation of China under Grant No. 81227901, 81371594, 61302024, 81527805, and 61231004.

## REFERENCES

- [1] Liu HG, Ren G, Miao Z, Zhang XF, Tang X, Han PZ, Gambhir SS, Cheng Z. Molecular optical imaging with radioactive probes. *PLoS ONE*. 2010;5:e9470.
- [2] Thorek DL, Das S, Grimm J. Molecular imaging using nanoparticle quenchers of Cerenkov luminescence. *Small*. 2014;10:3729-3734.
- [3] Ruggiero A, Holland JP, Lewis JS, Grimm J. Cerenkov luminescence imaging of medical isotopes. *J Nucl Med*. 2010;51:1123–1130.
- [4] Spinelli AE, Boschi F. Novel biomedical applications of Cerenkov radiation and radioluminescence imaging. *Phys Med*. 2015;31:120-129.
- [5] Zhang X, Kuo C, Moore A, Ran C. Cerenkov luminescence imaging of interscapular brown adipose tissue. *J Vis Exp*. 2014;(92):e51790.
- [6] Balkin ER, Kenoyer A, Orozco JJ, Hernandez A, Shadman M, Fisher DR, Green DJ, Hylarides MD, Press OW, Wilbur DS, Pagel JM. In vivo localization of <sup>90</sup>Y and <sup>177</sup>Lu radioimmunoconjugates using Cerenkov luminescence imaging in a disseminated murine leukemia model. *Cancer Res*. 2014;74:5846-5854.
- [7] Timmermand OV, Tran TA, Strand SE, Axelsson J. Intratherapeutic biokinetic measurements, dosimetry parameter estimates, and monitoring of treatment efficacy using cerenkov luminescence imaging in preclinical radionuclide therapy. *J Nucl Med*. 2015;56:444-449.
- [8] Steinberg JD, Raju A, Chandrasekharan P, Yang CT, Khoo K, Abastado JP, Robins EG, Townsend DW. Negative contrast Cerenkov luminescence imaging of blood vessels in a tumor mouse model using [68Ga]gallium chloride. *EJNMMI Res*. 2014;4:1.
- [9] Spinelli AE, Lo MS, Calandrino R, Sbarbati A, Boschi F. Optical imaging of Tc-99m-based tracers: in vitro and in vivo results. *J Biomed Opt*. 2011;16:275-277.
- [10] Thorek DL, Riedl CC, Grimm J. Clinical Cerenkov luminescence imaging of <sup>18</sup>F-FDG. *J Nucl Med*. 2014;55:95-98.
- [11] Liu H, Carpenter CM, Jiang H, Pratz G, Sun C, Buchin MP, Gambhir SS, Xing L, Cheng Z. Intraoperative imaging of tumors using Cerenkov luminescence endoscopy: a feasibility experimental study. *J Nucl Med*. 2012;53:1579-1584.
- [12] Carpenter CM, Ma X, Liu H, Sun C, Pratz G, Wang J, Gambhir SS, Xing L, Cheng Z. Cerenkov luminescence endoscopy: improved molecular sensitivity with  $\beta^-$ -emitting radiotracers. *J Nucl Med*. 2014;55:1905-1909.
- [13] Kothapalli SR, Liu H, Liao JC, Cheng Z, Gambhir SS. Endoscopic imaging of Cerenkov luminescence. *Biomed Opt Express*. 2012;3:1215-1225.
- [14] Bernhard Y, Collin B, Decréau RA. Inter/intramolecular Cherenkov radiation energy transfer (CRET) from a fluorophore with a built-in radionuclide. *Chem Commun*. 2014;50:6711-6713.
- [15] Dothager RS, Goiffon RJ, Jackson E, et al. Cerenkov radiation energy transfer (CRET) imaging: A novel method for optical imaging of PET isotopes in biological systems. *PLoS ONE*. 2010;5:e13300.
- [16] Joanne L, Dobrucki LW, Marina M, Chaney EJ, Suslick KS, Boppart SA.

Enhancement and wavelength-shifted emission of Cerenkov luminescence using multifunctional microspheres. *Phys Med Biol.* 2015;60:727-739.

[17] Thorek DL, Ogirala A, Beattie BJ, Grimm J. Quantitative imaging of disease signatures through radioactive decay signal conversion. *Nat Med.* 2013;19:1345-1350.

[18] Hu Z, Liang J, Yang W, Fan W, Li C, Ma X, Chen X, Ma X, Li X, Qu X, Wang J, Cao F, Tian J. Experimental Cerenkov luminescence tomography of the mouse model with SPECT imaging validation. *Opt Express.* 2010;18:24441-24450.

[19] Li C, Mitchell GS, Cherry SR. Cerenkov luminescence tomography for small animal imaging. *Opt Lett.* 2010;35:1109-1111.

[20] Ding X, Wang K, Jie B, Luo Y, Hu Z, Tian J. Probability method for Cerenkov luminescence tomography based on conformance error minimization. *Biomed Opt Express.* 2014;5:2091-2112.

[21] H. Liu, X. Yang, T. Song, C. Bao, L. Shi, Z. Hu, K. Wang, J. Tian. Multispectral hybrid Cerenkov luminescence tomography based on the finite element SPn method. *J Biomed Opt.* 2015;20:086007.

[22] Z. Hu, X. Ma, X. Qu, W. Yang, J. Liang, J. Wang, J. Tian. Three-dimensional noninvasive monitoring iodine-131 uptake in the thyroid using a modified Cerenkov luminescence tomography approach. *PLoS ONE.* 2012;7:e37623.

[23] AE Spinelli, C Kuo, BW Rice, R Calandrino, P Marzola, A Sbarbati, F Boschi. Multispectral Cerenkov luminescence tomography for small animal optical imaging. *Opt Express.* 2011;19:12605–12618.

[24] Z. Hu, Y. Qu, K. Wang, X. Zhang, J. Zha, T. Song, C. Bao, H. Liu, Z. Wang, J. Wang, Z. Liu, H. Liu, J. Tian. In vivo nanoparticle-mediated radiopharmaceutical-excited fluorescence molecular imaging. *Nat Commun.* 2015;6:7560.



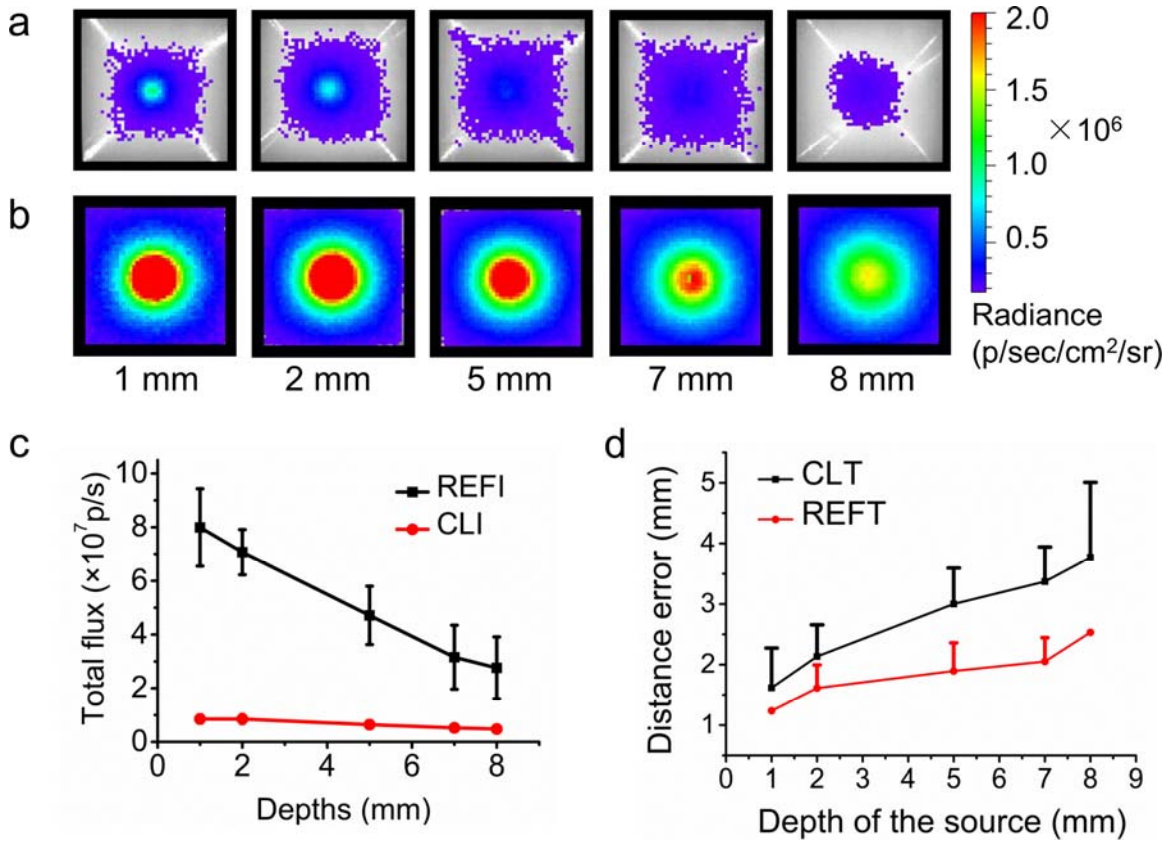


FIGURE 2. CLI and REFI of the phantoms. (a) Cerenkov luminescence images of phantoms injected with  $^{68}\text{Ga}$  with radioactivity of  $5 \mu\text{Ci}$ . Depths of the sources were 1 mm, 2 mm, 5 mm, 7 mm and 8 mm, respectively. (b) Radioluminescent images of 1 mg of EO excited by  $^{68}\text{Ga}$  with the radioactivity of  $5 \mu\text{Ci}$ . (c) The quantification comparison results of REFI and CLI. (d) The comparison of the 3D reconstruction distance errors of CLT and REFT.

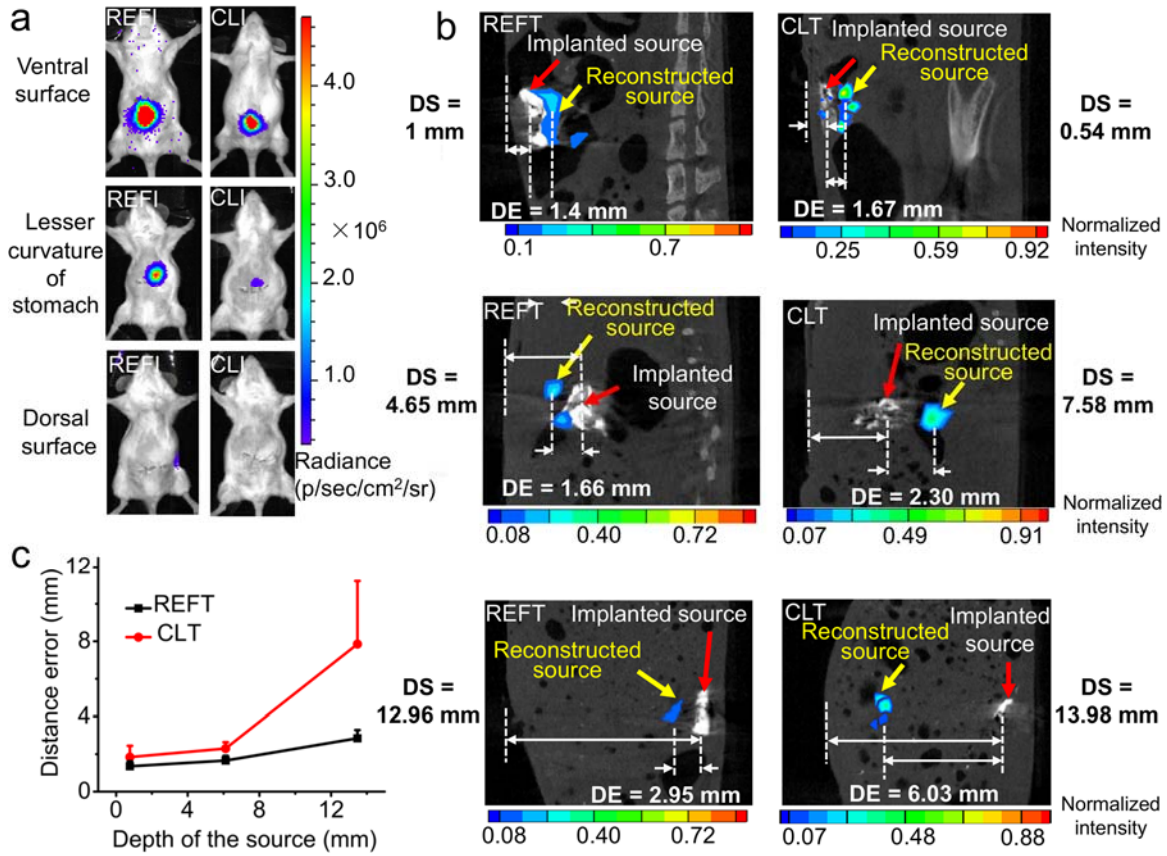


FIGURE 3. REFT and CLT of the artificial source-implantation mouse models. (a) REFI (left) and CLI (right) of the mice implanted with artificial sources, respectively. The position of the implanted source was close to the ventral surface of the abdomen (the first row), the lesser curvature of the stomach (the second row) and the dorsal surface of the abdomen of the mouse (the third row), respectively. (b) Comparison of reconstruction results of REFT and CLT. DS means the source depth from the real source position to the surface of mouse body. DE means the reconstructed distance error, which is defined as the distance from the real source position to the reconstructed source position. (c) The relationship between the distance error of REFT or CLT and the depth of the implanted sources.

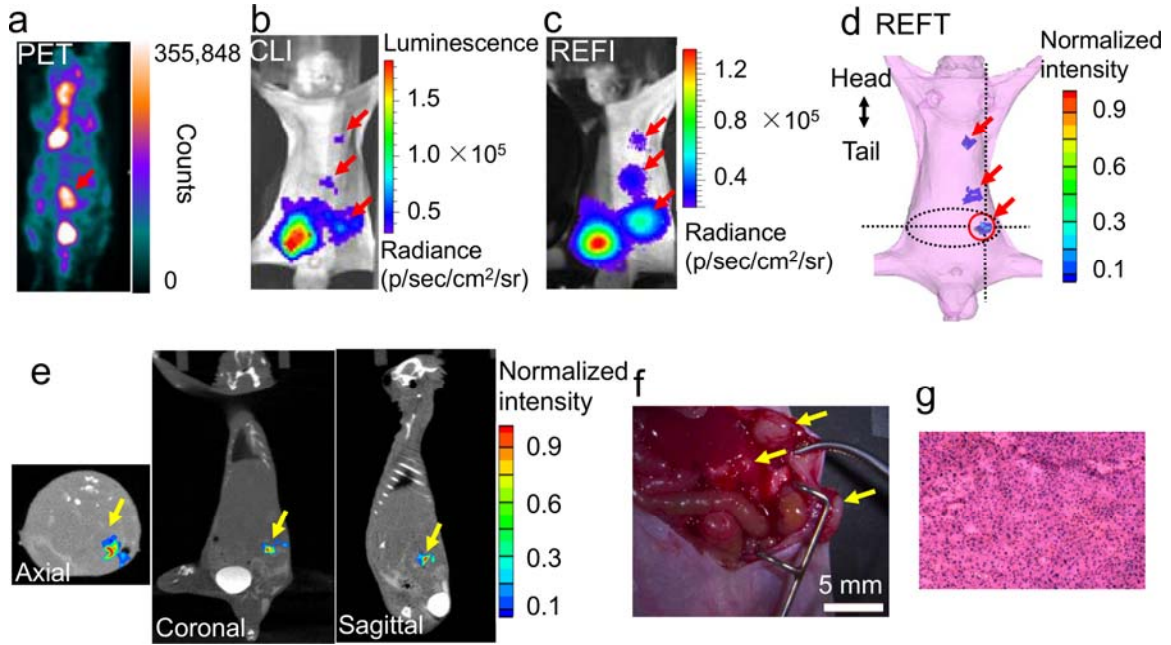


FIGURE 4. Small animal PET, CLI, REFI, and REFT of the mouse bearing HCC tumors. (a)-(d) Small animal PET, CLI, REFI, and REFT of the same mouse. (e) The axial, coronal and sagittal view of reconstructed results of REFT, respectively. (f) The photograph of the three tumors during the operation of the mouse. (g) H&E results of the tumors.

Table 1 Comparison of detection rates of REFT and PET.

	Detection rate of REFT (%)	Detection rate of PET (%)
Mouse 1	100	33.3
Mouse 2	80	60
Mouse 3	100	50
Mouse 4	75	25
Mean	88.75	42.08
SD	13.15	15.84